# Exploiting the dispersion of the double-negative-index fishnet metamaterial to create a broadband low-profile metallic lens

**B. Orazbayev,[1] V. Pacheco-Peña,[1] M. Beruete,[1] and M. Navarro-Cía,[2,3,4,*]**

[1]*Antennas Group-TERALAB, Universidad Pública de Navarra, Pamplona 31006, Spain*
[2]*Optical and Semiconductor Devices Group, Department of Electrical and Electronic Engineering, Imperial College London, London, SW7 2BT, UK*
[3]*Centre for Plasmonics and Metamaterials, Imperial College London, London, SW7 2AZ, UK*
[4]*Centre for Terahertz Science and Engineering, Imperial College London, London, SW7 2AZ, UK*
[*] *m.navarro@imperial.ac.uk*

**Abstract:** Metamaterial lenses with close values of permittivity and permeability usually display low reflection losses at the expense of narrow single frequency operation. Here, a broadband low-profile lens is designed by exploiting the dispersion of a fishnet metamaterial together with the zoning technique. The lens operates in a broadband regime from 54 GHz to 58 GHz, representing a fractional bandwidth ~7%, and outperforms Silicon lenses between 54 and 55.5 GHz. This broadband operation is demonstrated by a systematic analysis comprising Huygens-Fresnel analytical method, full-wave numerical simulations and experimental measurements at millimeter waves. For demonstrative purposes, a detailed study of the lens operation at two frequencies is done for the most important lens parameters (focal length, depth of focus, resolution, radiation diagram). Experimental results demonstrate diffraction-limited ~0.5λ transverse resolution, in agreement with analytical and numerical calculations. In a lens antenna configuration, a directivity as high as 16.6 dBi is achieved. The different focal lengths implemented into a single lens could be potentially used for realizing the front end of a non-mechanical zoom millimeter-wave imaging system.

©2015 Optical Society of America

**OCIS codes:** (050.1965) Diffractive lenses; (160.3918) Metamaterials; (350.3618) Left-handed materials.

## References and links

1. W. E. Kock, "Metal-Lens Antennas," Proc. IRE **34**, 828–836 (1946).
2. W. E. Kock, "Metallic Delay Lenses," Bell Syst. Tech. J. **27**(1), 58–82 (1948).
3. J. Brown, "Artificial dielectrics having refractive indices less than unity," Proc. IEE - Part IV Inst. Monogr. 51 – 62 (1953).
4. R. Marqués, F. Martín, and M. Sorolla, *Metamaterials with Negative Parameters: Theory, Design and Microwave Applications* (John Wiley & Sons, 2008).
5. L. Solymar and E. Shamonina, *Waves in Metamaterials* (Oxford University Press, 2009).
6. J. B. Pendry, "Negative Refraction Makes a Perfect Lens," Phys. Rev. Lett. **85**(18), 3966–3969 (2000).
7. N. Fang, H. Lee, C. Sun, and X. Zhang, "Sub-diffraction-limited optical imaging with a silver superlens," Science **308**(5721), 534–537 (2005).
8. Z. Liu, H. Lee, Y. Xiong, C. Sun, and X. Zhang, "Far-field optical hyperlens magnifying sub-diffraction-limited objects," Science **315**(5819), 1686 (2007).
9. V. V. Shevchenko, "The geometric-optics theory of a plane chiral-metamaterial lens," J. Commun. Technol. Electron. **54**(6), 662–666 (2009).
10. A. Demetriadou and Y. Hao, "A Grounded Slim Luneburg Lens Antenna Based on Transformation Electromagnetics," IEEE Antennas Wirel. Propag. Lett. **10**, 1590–1593 (2011).
11. M. Navarro-Cía, M. Beruete, M. Sorolla, and N. Engheta, "Lensing system and Fourier transformation using epsilon-near-zero metamaterials," Phys. Rev. B **86**(16), 165130 (2012).
12. R. S. Penciu, M. Kafesaki, T. Koschny, E. N. Economou, and C. M. Soukoulis, "Magnetic response of nanoscale left-handed metamaterials," Phys. Rev. B **81**(23), 235111 (2010).

#229395 - $15.00 USD Received 9 Dec 2014; accepted 19 Jan 2015; published 26 Mar 2015
© 2015 OSA

13. M. Beruete, M. Navarro-Cía, M. Sorolla, and I. Campillo, "Planoconcave lens by negative refraction of stacked subwavelength hole arrays," Opt. Express **16**(13), 9677–9683 (2008).
14. M. Navarro-Cía, M. Beruete, M. Sorolla, and I. Campillo, "Converging biconcave metallic lens by double-negative extraordinary transmission metamaterial," Appl. Phys. Lett. **94**(14), 144107 (2009).
15. M. Navarro-Cía, M. Beruete, I. Campillo, and M. S. Ayza, "Beamforming by Left-Handed Extraordinary Transmission Metamaterial Bi- and Plano-Concave Lens at Millimeter-Waves," IEEE Trans. Antenn. Propag. **59**(6), 2141–2151 (2011).
16. P. F. Goldsmith, "Zone plate lens antennas for millimeter and submillimeter wavelengths," in *The Third International Symposium on Space Terahertz Technology: Symposium Proceedings* (1992), pp. 345–361.
17. I. V. Minin and O. V. Minin, *Diffractional Optics of Millimetre Waves* (CRC Press, 2004).
18. H. D. Hristov, *Fresnel Zones in Wireless Links, Zone Plate Lenses and Antennas* (Artech House, 2000).
19. V. Pacheco-Peña, B. Orazbayev, V. Torres, M. Beruete, and M. Navarro-Cía, "Ultra-compact planoconcave zoned metallic lens based on the fishnet metamaterial," Appl. Phys. Lett. **103**(18), 183507 (2013).
20. V. Pacheco-Peña, B. Orazbayev, M. Beruete, and M. Navarro-Cía, "Zoned Near-Zero Refractive Index Fishnet Lens Antenna: Steering Millimeter Waves," J. Appl. Phys. **115**(12), 124902 (2014).
21. X. Chen, T. M. Grzegorczyk, B.-I. Wu, J. Pacheco, Jr., and J. A. Kong, "Robust method to retrieve the constitutive effective parameters of metamaterials," Phys. Rev. E Stat. Nonlin. Soft Matter Phys. **70**(1), 016608 (2004).
22. M. Navarro-Cía, M. Beruete, I. Campillo, and M. Sorolla, "Enhanced lens by ε and μ near-zero metamaterial boosted by extraordinary optical transmission," Phys. Rev. B **83**(11), 115112 (2011).
23. D. F. Filipovic and G. M. Rebeiz, "Double-slot antennas on extended hemispherical and elliptical quartz dielectric lenses," Int. J. Infrared Millim. Waves **14**(10), 1905–1924 (1993).
24. N. Llombart, G. Chattopadhyay, A. Skalare, and I. Mehdi, "Novel Terahertz Antenna Based on a Silicon Lens Fed by a Leaky Wave Enhanced Waveguide," IEEE Trans. Antenn. Propag. **59**(6), 2160–2168 (2011).
25. D. L. Runyon, "Optimum directivity coverage of fan-beam antennas," IEEE Antennas Propag. Mag. **44**(2), 66–70 (2002).

## 1. Introduction

Dielectric lenses have been designed for centuries, constrained to the permittivity values available in natural materials. In the 1940s, however, Kock devised lenses for microwaves made of metals [1,2], after realizing that an arrangement of metallic elements enables tailoring the effective permittivity, and thus its effective index to even less than unity values [3]. This introduced more freedom to the design, leading to converging lenses with plano-concave profiles. Another breakthrough in the field of lenses came after the inception of metamaterials, and their ability to tailor effective indices via manipulation of both ε and μ [4,5]. Metamaterials allow designing lenses with effective negative refractive index, which opens great opportunities, such as perfect lenses [6], superlenses [7], hyperbolic lenses [8], chiral lenses [9], transformation optics lenses [10] and lenses inspired on the energy squeezing principle [11]. Using metamaterial concepts, lenses with good (theoretically perfect) impedance matching to free space can be obtained, unlike classical metallic lenses and most dielectric lenses commercially available. As a side effect, they are usually limited to narrow bandwidths because of their highly dispersive nature. The good impedance matching property though removes the need of anti-reflection coatings that, at millimeter-waves, are not practical because of their thickness, weight, and cost.

Among all practical realizations of metamaterial lenses, the fishnet metamaterial, i.e., stacked subwavelength hole arrays, has become the strongest candidate for frequencies beyond microwaves because of its lower losses and frequency-robust magnetic response [12]. Hence, plano- and bi-concave fishnet lenses have been designed for millimeter-wave applications [13–15]. They show a good performance but are still relatively voluminous and heavy. These drawbacks can be overcome by applying the time-honored zoning technique, whereby redundant wavelength phase shift material is removed [1,16,17]. Alike zoned metallic [1] and optical dielectric lenses, also known as Fresnel lenses [17,18], this modification results in a fishnet metamaterial lens with low profile and, therefore, reduced weight and absorption losses [19,20]. The outcome is then a diffractive optical element akin to Fresnel zoned metallic plate lenses [17,18], but with an enhanced impedance matching.

In this paper we design a broadband zoned fishnet lens using an improved zoning technique, which involves a lens profile optimization for broadband performance. The strong dispersion of metamaterials in general, and the fishnet in particular, has been usually considered as a handicap in the past [4,5,13,15,19]. Here, dispersion is a key ingredient along

#229395 - $15.00 USD Received 9 Dec 2014; accepted 19 Jan 2015; published 26 Mar 2015
© 2015 OSA

with the zoning technique to build the zoned fishnet metamaterial lens operating in a wide band within the V-band of the millimeter-waves. The performance of the lens is investigated experimentally at two frequencies within the band at which the proposed lens outperforms Si lenses in terms of impedance matching and the results are compared against analytical calculations based on the Huygens-Fresnel principle, and full-wave numerical simulations.

## 2. Zoned fishnet metamaterial lens design

### *2.1 Fishnet metamaterial dispersion*

The fishnet metamaterial used in this work has a unit cell with the following dimensions: $d_x$ = 2.5 mm, $d_y$ = 5 mm, $d_z$ = 1.5 mm; and a thickness of the metallic plate $w$ = 0.5 mm (Fig. 1(a)). The index of refraction for an infinite number of plates (i.e., the bulk refractive index) is calculated using the Eigenmode solver of the commercial software CST Microwave Studio™, applying periodic boundary conditions in all planes. In this analysis the metal is modeled as perfect electric conductor. As shown in Fig. 1(a), the effective bulk refractive index is negative between 53 and 58 GHz and strongly dispersive. Meanwhile, the effective refractive index of finite structures is obtained using the standard retrieval method from the S-parameters [21], which are obtained with the frequency domain solver of CST Microwave Studio™, using now unit cell boundary conditions and modelling the metal as aluminum ($\sigma_{Al}$ = $3.56 \times 10^7$ S/m). The effective refractive index for several plates is shown in Fig. 1(a). As observed in Fig. 1(a), for two plates the effective index (dash-dot blue line) deviates from the infinite structure calculation due to the inhomogeneity of the fishnet metamaterial. The deviation between $q$ and $q$ + 1 stacked plates, and obviously with $q \to \infty$, is rapidly reduced with the number of plates and beyond $q$ = 4 stacked plates (dashed red line), there is a good convergence, specially within the range 54-56 GHz. Hereby it can be concluded that a relatively large number of plates is preferable to minimize the deviations of the effective refractive index with the number of stacked plates. However, this would result in undesirable increased thickness and losses. From previous experience, a starting stack of 4 plates is a good trade-off [13–15,19,22] to maintain thickness and losses low while the effective refractive index is not significantly altered with the addition of the few more stacked plates to reach the necessary profile.

### *2.2 Broadband lens analysis and final design*

The smooth zoned lens profile is found by applying the zoning technique. The zoning procedure implies the removal of layers each time a 2π phase shift is reached. The thickness of the layer t can be calculated as [1]:

$$t = \frac{\lambda_0}{1-n} \tag{1}$$

where $\lambda_0$ is the free-space wavelength and $n$ is the index of refraction of the medium. By combining Eq. (1) with the general equation of a conical [15], the design equation is as follows [19]:

$$\left(1-n_{lens}^2\right)\left(z+mt\right)^2 - 2\left(FL+mt\right)\left(1-n_{lens}\right)\left(z+mt\right)+x^2 = 0 \tag{2}$$

where $n_{lens}$ is the effective refractive index of the structure, $FL$ is the focal length, and m is an integer ($m$ = 0, 1, 2, 3) that represents the successive steps for the zoned lens profile. The successive steps for the zoned lens profile and thickness limits for two demonstrative frequencies are shown in Fig. 1(b). Given the discretization imposed by $d_x$ and $d_z$, the zoned yet smooth profile should be approximated by a staircase profile (see Fig. 1(b)). To obtain the optimal lens profile, which provides the broadband performance, a best fitting procedure to minimize the root-mean-square-error (RMSE) between the smooth profile and the staircase approximation is done for the whole operation band. Notice that the effective refractive index of an infinite fishnet metamaterial is used for this analysis. Due to the intrinsic dispersion of

#229395 - $15.00 USD Received 9 Dec 2014; accepted 19 Jan 2015; published 26 Mar 2015
© 2015 OSA

the fishnet structure, each frequency has only a unique optimal profile. So, for broadband operation a trade-off solution must be found. The resulting RMSE for this optimal profile is plotted in Fig. 1(c) as a function of frequency/effective bulk refractive index and focal length. From Fig. 1(c) it can be seen that RMSE has low values for the whole spectral window of interest demonstrating broadband regime. Therefore, as a result of this smart engineering procedure – combination of zoning technique and dispersion – the optimal zoned lens profile is obtained, see Fig. 1(b) (solid black curve). It should be noticed that the resulting lens profile is completely different from that used in previous works [19,20], where it was obtained by applying the zoning technique only for a single frequency. Figure 1(c) shows that the relative minimum of the RMSE follows a parabolic-like trend starting from $FL$ = 41 mm at 53 GHz and reaching the top end of the color map $FL$ = 65 mm around 58 GHz. This trend is a direct consequence of the strong dispersion of the fishnet metamaterial (see Fig. 1(a)) that causes chromatic aberration for the fishnet lens [13–15]. According to Fig. 1(c), the absolute minimum RMSE is obtained for $f$ = 53.5 GHz and $FL$ = 45 mm. However, from Fig. 1(a) we know that the convergence of the effective bulk refractive index for infinite and finite numbers of plates is poor at that frequency. Therefore, poor performance at this frequency is expected. Observing the figure, it is noticed that the best convergence happens in the interval 54-56 GHz. For this reason, in the next studies the frequencies at approximately both ends $f_1$ = 54 GHz and $f_2$ = 55.5 GHz are chosen for illustrative purposes. At these frequencies, the effective bulk refractive index is $n_{lens1}$ = –0.78 and $n_{lens2}$ = –0.43, respectively.

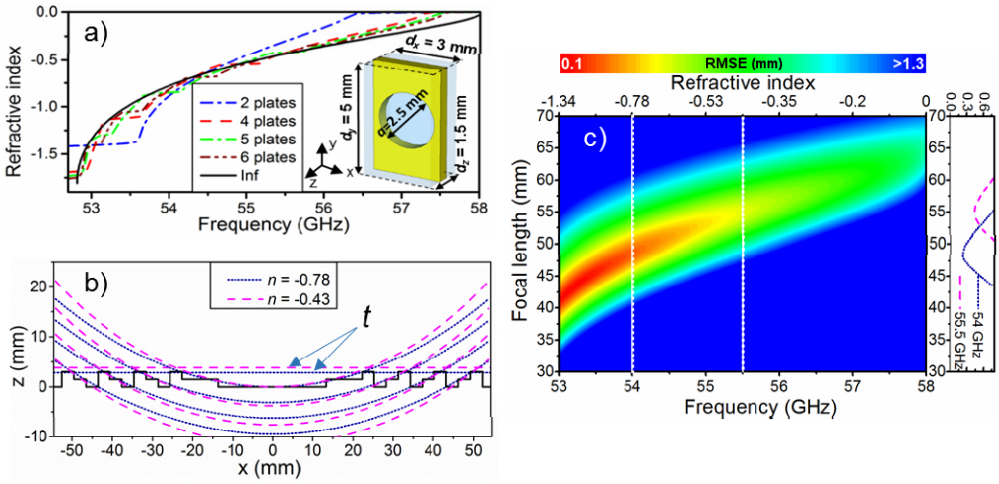


Fig. 1. (a) Effective refractive index, $n_z$, for a fishnet metamaterial made of 2 (blue dashed-dot curve), 4 (red dashed curve), 5 (green dashed-dot curve), 6 (brown dashed-dot-dot curve) and infinite number of plates (black solid curve). Dimensions of fishnet metamaterial unit cell (Inset); (b) Lens profiles and curves of the successive steps for: $n_{lens1}$ = –0.78 (dotted blue curve) and for $n_{lens2}$ = –0.43 (dashed pink curve) along with the values of the thickness limits, $t_1$ and $t_2$ (blue and pink horizontal curves, respectively); (c) color map of RMSE of the zoned lens profile as a function of frequency and focal length. The vertical dotted white lines indicate the frequencies whose associated RMSE are plotted on the on the right-hand side graph: $f_1$ = 54 GHz (dotted blue curve) and $f_2$ = 55.5 GHz (dashed pink curve).

At $f_1$ = 54 GHz and focal length $FL_1$ = 48.7 mm (8.8$\lambda_1$) the RMSE is $\delta_1$ = 0.22 mm. Such error can lead to a shift of the focus $\delta FL_1$ = - 0.7 mm (0.23$\lambda_1$ ≈2%) because of the staircase approximation imposed by the fishnet metamaterial. At the second frequency $f_2$ = 55.5 GHz and focal length $FL_2$ = 55 mm (10.2$\lambda_2$) the RMSE is $\delta_2$ = 0.44 mm and may result in a slightly larger focus shift $\delta FL_2$ = - 2.3 mm (0.4$\lambda_2$ ≈4%). The curves defined by Eq. (2) for four successive steps ($m$ = 0, 1, 2, 3) at the two considered frequencies are shown in Fig. 1(b): $f_1$, dotted blue lines; $f_2$, dashed pink lines. Also, the maximum thickness [1,19,20] for each

#229395 - $15.00 USD Received 9 Dec 2014; accepted 19 Jan 2015; published 26 Mar 2015
© 2015 OSA

frequency, $t_1$ = 2.8 mm (0.5$\lambda_1$ ≈2 $d_z$) and $t_2$ = 3.8 mm (0.7$\lambda_2$), are represented by horizontal dashed blue and pink lines, respectively.

Since one and two plates are necessary to realize the three-level binary profile, see Fig. 1(b), and four plates are the minimum for the central part (due to inhomogeneity of fishnet metamaterial), the total thickness of the lens results in $5d_z + w$ = 8 mm (1.4$\lambda_1$). Along $x$ and $y$ directions the structure consists of 37 $d_x$ and 27 $d_y$ periods, respectively. Therefore, the final design has the total dimensions 111 mm × 135 mm × 8 mm (19.8$\lambda_1$ × 24.1$\lambda_1$ × 1.4$\lambda_1$) without the frame used to facilitate the assembly. The fabricated zoned fishnet metamaterial lens is shown in Fig. 2.

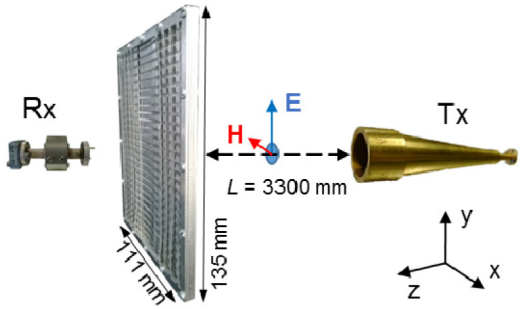


Fig. 2. Sketch of the experimental setup. Tx and Rx stand for transmitter and receiver, respectively.

## 3. Results

### *3.1 Analytical calculations*

First, in order to verify the design and estimate the focal positions, an analytical calculation is done by means of the Huygens-Fresnel principle for the two-dimensional case. This principle implies that each point of a wavefront acts as a secondary wave source. Given the holey nature of the fishnet, the point sources are located at the position of each hole of the input plate. For simplicity we neglect any kind of reflections and absorption. Furthermore, all sources have the same amplitude and radiate vertically polarized ($E_y$) cylindrical waves. The lens is assumed to be made from isotropic dispersive material with refractive index $n(f)$ corresponding to effective bulk refractive index $n_{lens}(f)$ of the fishnet metamaterial (Fig. 1(a)). The phase of each source is calculated as a sum of an incident wave phase and a phase shift in the lens. Then the resulting field in each point of space ($x$, $y$) is calculated by adding the fields of all sources. Mathematically, this can be written as:

$$A_{x,y} = \sum_{i=1}^{37} \frac{A_i}{\sqrt{l(x,y)}} e^{j(k_0 l(x,y) + k_0 n(f) d_i + \varphi_0)}$$
$$l(x,y) = \sqrt{(x - x_i)^2 + (y - y_i)^2} \quad (3)$$

where $A_i$ is amplitude of point source $i$; $l(x,y)$ is the distance between the point source $i$ and point in the space $(x,y)$; $k_0$ is the wave vector in free space; $x_i$, $y_i$ are the position coordinates of the holes; $n(f)$ is the effective bulk refractive index of the lens; $f$ is the operation frequency; $d_i$ is the path inside the lens; $\varphi_0$ is the phase of incident plane wave. First, the power distribution is calculated as a function of frequency and position along the optical axis of the lens (Fig. 3(a)).

A broadband operation is observed, with a band extending from 53.5 GHz ($FL$ = 45 mm) to 58 GHz ($FL$ = 56 mm) with the absolute maximum power located between 54 and 56 GHz, in good agreement with the RMSE calculation. In Fig. 3(a) one can notice that, alike other

#229395 - $15.00 USD Received 9 Dec 2014; accepted 19 Jan 2015; published 26 Mar 2015
© 2015 OSA

diffractive optical elements [17,18], there are secondary foci. For the frequency span shown, a secondary focus moving within the *z*-range 20 to 35 mm is visible. This secondary focus is however significantly lower in amplitude than the main focus. Next, the spatial power distribution on the *xz*-plane calculated using the Huygens-Fresnel principle for the two frequencies is presented in Fig. 4(a): $f_1$ = 54 GHz (top) and $f_2$ = 55.5 GHz (bottom). For both frequencies, clear foci can be observed with around half-wavelength transverse dimensions. Also, prominent side lobes are noticeable off-axis surrounding the focus. Nevertheless, they emerge at significant different distance than the focal plane.

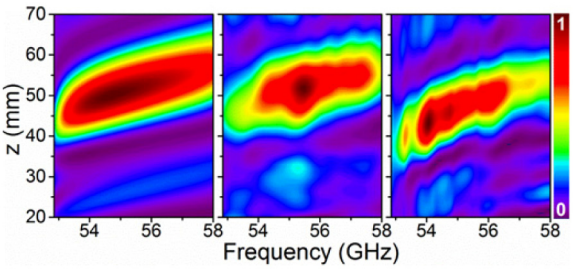


Fig. 3. Power distribution along *z* axis for the frequency range 52–58 GHz: (a) analytical results, (b) experimental and (c) simulation results.

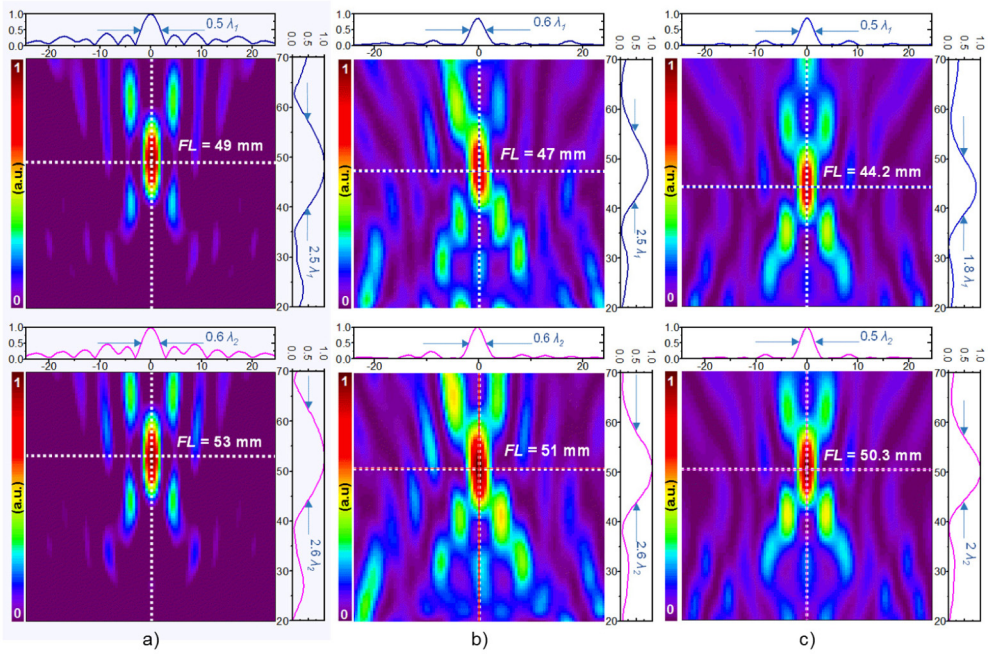


Fig. 4. Analytical (a), experimental (b) and simulation results (c) for of the spatial power distribution on the *xz*-plane for: (top) $f_1$ = 54 GHz and (bottom) $f_2$ = 55.5 GHz. The normalized power distributions along *x*-axis (at each focal length) and along the optical axis are represented in each panel on the top- and right-side plots, respectively.

### *3.2 Experimental results*

The experimental characterization is done using an AB Millimetre™ quasi-optical vector network analyzer with the setup illustrated in Fig. 2. To illuminate the lens, a V-band corrugated horn antenna is placed at a distance *L* = 3300 mm from the lens. At this distance the radius beam waist of the Gaussian beam is ~400 mm for both working frequencies, which

#229395 - $15.00 USD Received 9 Dec 2014; accepted 19 Jan 2015; published 26 Mar 2015
© 2015 OSA

ensures a uniform illumination of the lens. An open-ended rectangular waveguide (WR-15) is used as a detector, for the *xz* raster scanning. Millimeter-wave absorbers are used throughout the setup to mimic anechoic chamber conditions. The calibration is done by recording the transmitted power without the lens. For the power distribution as a function of frequency and *z* position, the lens is placed in the setup and the detector is moved from 20 to 70 mm away from the lens along *z*-axis (with 0.5 mm steps) while recording the spectrum in the range 50-60 GHz. Similarly, *z*-frequency- and *xz*-maps are generated experimentally using the prototype described previously (Fig. 2). Initially, the power distribution is obtained as a function of frequency and z position. The color map is shown in Fig. 3(b), which resembles that obtained following the Huygens-Fresnel principle (Fig. 3(a)). This color map is obtained after applying a Butterworth low pass filter, in order to minimize the ripples in the experimental data caused by the excitation of standing waves between the lens and the detector (demonstrated in the simulation results of next section but not shown here). In this figure, the broadband performance of the zoned lens from 54 GHz to 58 GHz can be observed, with some penalty in performance for extreme frequencies, which is in good agreement with the results obtained by the Huygens-Fresnel principle. The maximum power enhancement (i.e., the ratio between the intensity with and without lens for each *xz* position) is 10.5 dB at 54 GHz and 13.1 dB at 55.5 GHz. These maxima occur at $z$ = 47 mm and 51 mm, respectively. It is also noticeable a secondary focus at around 30 mm for 55 GHz. Further, the power is scanned on *xz*-plane at frequencies $f_1$ = 54 GHz and $f_2$ = 55.5 GHz. The results of the spatial power distribution are shown in Fig. 4(b), for $f_1$ (top) and $f_2$ (bottom), respectively. A good qualitative agreement with the analytical results is evident.

*3.3 Simulation results*

For completeness, a full-wave numerical analysis of the realistic 3D model of the zoned lens is done using the transient solver of the commercial software CST Microwave Studio™. The bulk conductivity of aluminum ($\sigma_{Al} = 3.56 \times 10^7$ S/m) is taken into account for the modeling of the fabricated fishnet metamaterial lens. A fine hexahedral mesh is used with minimum and maximum mesh cell sizes of 0.125 mm ($0.02\lambda_1$) and 0.28 mm ($0.05\lambda_1$), respectively. A vertically polarized ($E_y$) plane wave is used to excite the lens, impinging normally on its planar face. Perfectly matched layers ("open add space") are used in the boundaries of the simulation box to emulate a lens in free space. Given the two-fold symmetry of the problem, electric and magnetic mirror planes are placed in the *xz*- and *yz*-planes, respectively, with the aim to reduce computation time. The simulation is run for a sufficiently long time to ensure that the continuous-wave information computed by Fourier transformations is valid. Although time consuming, and thus, undesirable for a fast prototyping (unlike the Huygens-Fresnel principle), the results derived from this approach should obviously have a better agreement with the experimental ones.

Initially, the power distribution as a function of *z* position and frequency is obtained by placing *E*-field and *H*-field probes, instead of an open-ended WR-15, along the optical axis (*z*-axis) with a 0.5 mm step. These probes record the waveform at their positions and by Fourier transformation, the *E*- and *H*-field spectra are obtained. The resulting power distribution is shown in Fig. 3(c). The focal spot is located in the frequency range 53.5-56.5 GHz and moving from 42 up to 51.5 mm along *z*-axis. This result resembles the analytical and experimental ones. Alike the experimental data, the dark red spot accounting for the maximum power is concentrated within a narrower frequency band. Likewise, the preceding secondary focus vanishes at 56.5 GHz. These features were not captured by the analytical calculation of Fig. 3(a).

Next, in order to confirm the broadband performance of the zoned lens, the enhancement as a function of frequency is compared to the enhancement of a zoned fishnet metamaterial lens optimized for single-band operation, already reported in our previous works [19,20]. The numerical results are shown in Fig. 5(a) and are obtained using the same full-wave numerical analysis of the realistic 3D model. The zoned lens introduced here exhibits an enhancement above 9 dB for the whole negative refractive index band and has a maximum at the frequency

#229395 - $15.00 USD Received 9 Dec 2014; accepted 19 Jan 2015; published 26 Mar 2015
© 2015 OSA

$f_1$ = 54 GHz, which is in good agreement with Fig. 1(c) where RMSE is minimal at this frequency. The zoned lens optimized for single-band operation, in turn, achieves enhancement values above 9 dB only at the design frequency range, 55 - 56.5 GHz.

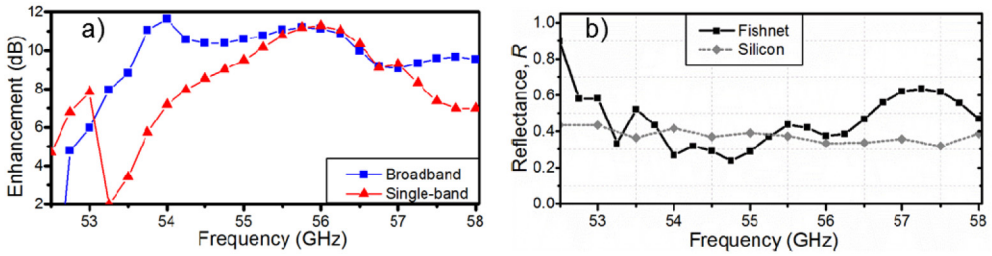


Fig. 5. (a) Numerical results for the enhancement as a function of frequency for the single-mode zoned lens (red curve) and for the broadband zoned lens (blue curve); (b) reflectance for the zoned fishnet metamaterial lens (solid black line) and the Silicon zoned lens (dashed grey line).

The *xz*-maps of power distribution generated from the simulation for $f_1$ = 54 GHz and $f_2$ = 55.5 GHz are plotted on the top and bottom color maps in Fig. 4(c), respectively. These color maps bear a resemblance to analytical and experimental results. In particular, they model more accurately than the analytical approach the relative amplitude between the main focus and the side lobes.

Finally, the free-space matching is estimated by obtaining the reflectance for the full structure. The reflectance $R$ is defined as the ratio of the reflected power $P_{refl}$ and the incident power $P_{inc}$, $R = P_{refl}/P_{inc}$. The incident flux $P_{inc}$ is calculated without the lens, in order to avoid any contribution of reflected power. The reflected power $P_{refl}$ is calculated from stationary power flux located before the lens $P_{st} = P_{inc} - P_{refl}$. Given the $z$ normal planes at which we compute $P_{st}$ and $P_{inc}$, and that the lens is illuminated with a linearly polarized plane wave, we consider only the $z$-component of the power flux. The obtained reflectance $R$ for the frequencies 52.5-58 GHz is shown in Fig. 5(b). As it is expected from the dispersion diagram (Fig. 1(a)), below 53 GHz the reflectance $R$ is significantly high. At the chosen illustrative frequencies, $R$ is 0.26 and 0.43 for the lower and higher frequency, respectively. One can notice the agreement with Fig. 3(c), where the maxima are at 54 GHz and 54.75 GHz. When comparing the reflectance of the zoned fishnet metamaterial lens with a zoned lens made of Silicon (dashed grey line), a material widely used for lenses at millimeter-waves and terahertz [23,24], it is evident that the lens introduced here outperforms the Silicon counterpart in terms of Fresnel reflection losses for ~54 – 55. 5 GHz. This frequency range coincides with the band where good convergence of effective refractive index among different number of stacked layers was observed, see Fig. 1.

### *3.4 Radiation properties: lens antenna*

Once the lens is fully characterized, we investigate its performance in a lens antenna configuration. An open-ended WR-15 is used now as a feeder placed at the experimentally-computed focal length of each frequency. Meanwhile, a high gain standard horn antenna is placed 3650 mm away from the flat face of the zoned lens to detect the radiated power. Notice that, strictly speaking, the detection is not done in far-field according to the convention $z_{ff} = 2D^2/\lambda$, where $D$ is the diameter of the lens: for $f_1$ = 54 GHz $z_{ff1}$ = 4435 mm and for $f_2$ = 55.5 GHz $z_{ff2}$ = 4560 mm. Nevertheless, it should give an approximated result. To measure the angular distribution of the radiated power, the feeder and the zoned lens stand on a rotating platform that rotates from –90 deg to + 90 deg with 1 deg step. Absorbing material is also used throughout the setup for reflection suppression. Co- and cross-polar angular measurements for $f_1$ = 54 GHz and $f_2$ = 55.5 GHz are displayed in Fig. 6. For $f_1$ (Fig. 6(top)), the main lobe has half-power beamwidth (HPBW) and first null beamwidth (FNBW) of 3.5 deg and 40 deg, respectively, with a side lobe level (SLL) of 5.7 dB at around ± 8 deg. It can

#229395 - $15.00 USD Received 9 Dec 2014; accepted 19 Jan 2015; published 26 Mar 2015
© 2015 OSA

be demonstrated that this side lobe corresponds to the (0,-1) grating lobe of the periodic holey pattern [20]. An additional minor lobe can be seen at ± 65 deg. In this case, it is caused by the spillover [20] and can potentially be eliminated by increasing the lateral size of the lens. The results for f2 (Fig. 6(bottom)) are similar. The main lobe has HPBW = 4.3 deg and FNBW = 39 deg, respectively, with SLL = 6.7 dB at around ± 7 deg. The spillover lobe occurs at ± 65 deg. The maximum directivity estimated using the method described in Ref [25]. is 16.6 dBi and 15.6 dBi for $f_1$ and $f_2$, respectively. The cross-polar level is ~25 dB and ~40 dB for $f_1$ and $f_2$ respectively, indicating the good performance of the zoned lens antenna. Arguably, the measured cross-polar level might be originated from experimental misalignment, since the on-axis cross-polar should vanish for a perfectly symmetric configuration about the *yz*-plane, as the simulations described below confirm. The non-negligible cross-polar measured at ± 65 deg arises evidently from the spillover.

Radiation parameters have also been modeled numerically. An open-ended WR-15 feeder is placed at the numerical focal length of each frequency and the radiation pattern is calculated at the same distance as in the experiment $z_{ff}$ = 3650 mm. The co-polar results are plotted as well in Fig. 6 to facilitate the comparison with the experiment. The numerical cross-polar, however, is not plotted given its negligible value. One can see that the radiation patterns for numerical calculations are similar to experimental results. The main lobe has HPBW = 3.2 deg and FNBW = 40 deg for $f_1$, and HPBW = 4.1 deg and FNBW = 56 deg for $f_2$. The first side lobes and the spillover lobe appear at similar angles, but with lower levels than in the experiment. The maximum directivity, which can be computed readily from the simulation, is 15.4 dBi for $f_1$ and 15.2 dBi for $f_2$, which is in good agreement with values estimated from experimental results.

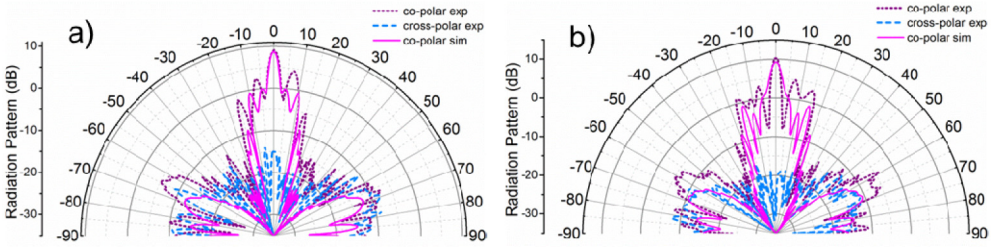


Fig. 6. H-plane (*xz*-plane) radiation pattern for: (top) $f_1$ = 54 GHz and (bottom) $f_2$ = 55.5 GHz. Dashed and solid lines represent experimental and numerical results, respectively. Purple and blue colors stand for co- and cross-polar data, respectively.

## 4. Discussion

To facilitate the comparison, all main focal properties for the three methods investigated are gathered in Table 1. It is shown that the results are also in good agreement quantitatively with each other and with the designed values based on ray tracing approximation. Only, the FWHM show minor disagreement between measurements and both analytical and numerical calculations. This can be arguably ascribed to the non-subwavelength nature of the detector used in the experiment (an open-ended waveguide, WR-15), which averages the field strength.

For the analytical results, the deviations of the focal positions from designed values are less than 2%, which is included into the error of the zoned lens profile. The experimental results show deviations of focal length below 6%. These discrepancies fall perfectly within the experimental error caused by misalignments and defects of the fabricated zoned lens. As for simulations, the deviations are less than 9.5%. It is worth noting that for the initial design based on ray tracing, the lens is assumed to be isotropic with refractive index extracted from the infinite-layered fishnet structure. Hence, it is reasonable to expect a good agreement between the experimental and numerical results, where the anisotropic nature of the fishnet is fully considered. The analytical results obtained applying the Huygens-Fresnel principle are

#229395 - $15.00 USD Received 9 Dec 2014; accepted 19 Jan 2015; published 26 Mar 2015
© 2015 OSA

more similar to the ray tracing design than the where the lens is assumed isotropic and, therefore, deviate from experimental and numerical results.

**Table 1. Results of the zoned lens**

| | $FL_1$[1], mm | $FL_2$, mm | $FWHM_1$[2],mm | $FWHM_2$,mm | $DF_1$[3], mm | $DF_2$, mm |
|---|---|---|---|---|---|---|
| Analytical | 49 | 53 | 3 | 3 | 14 | 13.8 |
| | $8.8\lambda_1$ | $9.8\lambda_2$ | $0.5\lambda_1$ | $0.6\lambda_2$ | $2.5\lambda_1$ | $2.6\lambda_2$ |
| Experimental | 47 | 51 | 3.3 | 3.4 | 13.7 | 14.2 |
| | $8.4\lambda_1$ | $9.4\lambda_2$ | $0.6\lambda_1$ | $0.6\lambda_2$ | $2.5\lambda_1$ | $2.6\lambda_2$ |
| Simulation | 44.2 | 50.3 | 2.8 | 2.8 | 10 | 10.7 |
| | $7.9\lambda_1$ | $9.3\lambda_2$ | $0.5\lambda_1$ | $0.5\lambda_2$ | $1.8\lambda_1$ | $2\lambda_2$ |

[1]FL is the focal length.
[2]FWHM is the full width at half maximum.
[3]DF is the depth of focus.

Thereby, the good agreement observed between all approaches validates the good performance of the lens for frequencies from 54 GHz to 58 GHz. Also, these results demonstrate that, despite all the assumptions used for the Huygens-Fresnel principle, it can be well used initially for a fast prototyping.

The analysis shown so far demonstrates that strong dispersion of the fishnet, usually considered as a drawback, can be turned into an advantage to design broadband diffractive optical devices. Additionally, the narrow band of the fishnet guarantees the filtering of the undesired frequencies, whereas the strong dispersion allows designing the lens with more than one narrow working frequency with different focal lengths suitable for non-mechanical zooming.

## 5. Conclusion

The basic aspects of designing a dual-band zoned fishnet metamaterial lens have been discussed. The strong dispersion of the fishnet, that otherwise would be a handicap, is here shown to be an advantage when combined with the zoning technique. A converging zoned fishnet metamaterial lens has been designed, fabricated and measured at the V-band of the millimeter-waves. Analytical, experimental and simulation results agree well, and have also good agreement with the designed values based on ray tracing. A lens antenna has been subsequently proposed. The numerical results are confirmed experimentally showing directivities above 15 dB for both frequency bands.

The low-profile and weight of the zoned lens together with its ability to operate in two nearby narrow bands with good free-space matching make it a good competitor to other diffractive optical devices made of dielectrics (which tend to be lossy and mismatched for millimeter and submillimeter-wave) or metals (which tend to be mismatched).

## Acknowledgments

In memoriam Prof. Mario Sorolla. This work was supported in part by the Spanish Government under contract Consolider Engineering Metamaterials CDS2008-00066 and contract TEC2011-28664-C02-01. B. O. is sponsored by Spanish Ministerio de Economía y Competitividad under grant FPI BES-2012-054909. V.P.-P. is sponsored by Spanish Ministerio de Educación, Cultura y Deporte under grant FPU AP-2012-3796. M. B. is sponsored by the Spanish Government via RYC-2011-08221. M. N.-C. is supported by the Imperial College Junior Research Fellowship.

#229395 - $15.00 USD Received 9 Dec 2014; accepted 19 Jan 2015; published 26 Mar 2015
© 2015 OSA